

Magnetically Assisted Vorticity Production in Decaying Acoustic Turbulence

AXEL BRANDENBURG^{1,2,3,4} AND EVAN SCANNAPIECO⁵

¹*Nordita, KTH Royal Institute of Technology and Stockholm University, Hannes Alfvéns väg 12, SE-10691 Stockholm, Sweden*

²*The Oskar Klein Centre, Department of Astronomy, Stockholm University, AlbaNova, SE-10691 Stockholm, Sweden*

³*McWilliams Center for Cosmology & Department of Physics, Carnegie Mellon University, Pittsburgh, PA 15213, USA*

⁴*School of Natural Sciences and Medicine, Ilia State University, 3-5 Cholokashvili Avenue, 0194 Tbilisi, Georgia*

⁵*School of Earth and Space Exploration, Arizona State University, P.O. Box 876004, Tempe, AZ 85287, USA*

(Received 2025, January 30; Revised 2025, March 4; Accepted 2025, March 5)

ABSTRACT

We study vorticity production in isothermal, subsonic, acoustic (nonvortical), and decaying turbulence due to the presence of magnetic fields. Using three-dimensional numerical simulations, we find that the resulting kinetic energy cascade follows the ordinary Kolmogorov phenomenology involving a constant spectral energy flux. The nondimensional prefactor for acoustic turbulence is larger than the standard Kolmogorov constant due to the inefficient dissipation of kinetic energy. We also find that the Lorentz force can drive vortical motions even when the initial field is uniform, by converting a fraction of the acoustic energy into vortical energy. This conversion is shown to be quadratic in the magnetic field strength and linear in the acoustic flow speed. By contrast, the direct production of vortical motions by a non-force-free magnetic field is linear in the field strength. Our results suggest that magnetic fields play a crucial role in vorticity production in cosmological flows, particularly in scenarios where significant acoustic turbulence is prevalent. We also discuss the implications of our findings for the early Universe, where magnetic fields may convert acoustic turbulence generated during cosmological phase transitions into vortical turbulence.

Keywords: Astrophysical magnetism (321) — Plasma astrophysics (1261)

1. INTRODUCTION

One can envisage diverse astrophysical situations where the velocity field is irrotational and the gas motions are predominantly acoustic. Such flows can be described as the gradient of a potential function, and thus may arise from gravitational accelerations or barotropic pressure fluctuations.

Vortical motions, on the other hand, arise hydrodynamically through shocks (Porter et al. 2015) and through the baroclinic term resulting from oblique gradients of density and pressure (Del Sordo & Brandenburg 2011; Federrath et al. 2011; Jahanbakhshi et al. 2015; Elias-López et al. 2023, 2024). However, the efficiency of these effects is limited because they depend on the Mach number, which is often small. Thus, thermal effects such as differential heating may be too weak to produce baroclinicity.

On the other hand, it has been known for some time that magnetic fields create vorticity regardless of the possible presence of irrotational turbulence as long as

the curl of the Lorentz force is nonvanishing. This was demonstrated by Kahniashvili et al. (2012), who were primarily interested in the effect of turbulence from cosmological phase transitions on an inflationary-generated magnetic field. Yet the possibility of producing vorticity in the presence of magnetic fields is more general and may also have occurred under other circumstances.

A characteristic property of vortical turbulence is the constancy of the energy flux from the driving scale along the turbulent cascade down to the dissipation scale. This allows one to express the energy spectrum in nondimensional form, yielding a dimensionless prefactor known as the Kolmogorov constant (Frisch 1995; Sreenivasan 1995), which is well measured in vortical turbulence.

There have been numerous studies of acoustic turbulence, starting with the early works of Kadomtsev & Petviashvili (1973), Elsasser & Schamel (1974, 1976), and L’vov & Mikhailov (1981). However, many subsequent studies focused on compressibil-

ity effects (Passot & Pouquet 1987; Shivamoggi 1992; Cho & Lazarian 2005; Galtier & Banerjee 2011). Although the spectral properties of acoustic turbulence have also been investigated in some detail (Falkovich & Meyer 1996; Kuznetsov & Krasnoselskikh 2008; Kochurin & Kuznetsov 2022; Ricard & Falcon 2023), no values for a Kolmogorov-like prefactor have been quoted for magnetized acoustic turbulence.

Here, we use numerical simulations to revisit magnetic vorticity production in acoustic turbulence, focusing on three main questions: (1) can the Kolmogorov prefactor be determined for acoustic turbulence, and how does the presence of a magnetic field change its value? (2) To what extent does magnetically modified acoustic turbulence resemble ordinary turbulence? (3) Can acoustic turbulence be converted into vortical turbulence due to the presence of a magnetic field?

We emphasize that we are not concerned with strong compressibility effects, which would occur at large Mach numbers (Schleicher et al. 2013; Federrath et al. 2014; Porter et al. 2015). This is why we prefer the term “acoustic” (Kadomtsev & Petviashvili 1973) over “compressive.” Furthermore, compared to the more general term “irrotational,” the term “acoustic” is more directly suggestive of low-amplitude subsonic flows.

The structure of this work is as follows. In §2 we describe the magnetohydrodynamic (MHD) equations and their implications for vorticity production, as well as our numerical approach, parameter space, and analysis techniques. In §3 we present our results, focusing on measurements of the Kolmogorov prefactor and magnetic vorticity production. Implications and conclusions are given in §4.

2. THE MODEL

2.1. Basic Equations

We solve the hydrodynamic and MHD equations with an isothermal equation of state, where the pressure p and density ρ are related to each other through $p = \rho c_s^2$ with $c_s = \text{const}$ being the isothermal speed of sound. This precludes vorticity production by the baroclinic term. The evolution equations for ρ and the velocity \mathbf{u} are then given by

$$\frac{D \ln \rho}{Dt} = -\nabla \cdot \mathbf{u}, \quad \text{and} \quad (1)$$

$$\frac{D\mathbf{u}}{Dt} = -c_s^2 \nabla \ln \rho + \frac{\mathbf{J} \times \mathbf{B}}{\rho} + \mathbf{F}_{\text{visc}}, \quad (2)$$

where \mathbf{B} is the magnetic field, $\mathbf{J} = \nabla \times \mathbf{B}/\mu_0$ is the current density with μ_0 being the vacuum permeability, $\mathbf{J} \times \mathbf{B}$ is the Lorentz force, $\mathbf{F}_{\text{visc}} = \rho^{-1} \nabla \cdot (2\nu \rho \mathbf{S})$ is the viscous force per unit mass with ν being the kinematic

viscosity, and \mathbf{S} the rate-of-strain tensor with components $S_{ij} = \frac{1}{2}(\partial_i u_j + \partial_j u_i) - \frac{1}{3} \delta_{ij} \nabla \cdot \mathbf{u}$. Note that our simulations only include the usual shear viscosity and assume that the bulk viscosity is absent; see Beattie et al. (2023) for a recent work on this aspect.

In simulations in which the magnetic field is included, we also solve for the magnetic potential \mathbf{A} via

$$\frac{\partial \mathbf{A}}{\partial t} = \iota \mathbf{u} \times \mathbf{B} + \eta \nabla^2 \mathbf{A}, \quad (3)$$

so that $\nabla \times \mathbf{A}$ is always divergence free. In several of our models, we also impose an external magnetic field \mathbf{B}_0 by writing $\mathbf{B} = \mathbf{B}_0 + \nabla \times \mathbf{A}$, so that we can adopt periodic boundary conditions on \mathbf{A} . In Equation (3), the parameter ι is introduced to allow us to turn off the induction term ($\iota = 0$). By default, we have $\iota = 1$.

2.2. Vorticity Production

To understand the terms leading to vorticity production, we take the curl of Equation (2) and find

$$\frac{\partial \mathbf{w}}{\partial t} = \nabla \times (\mathbf{u} \times \mathbf{w}) + \dot{\mathbf{w}}_{\text{mag}} + \dot{\mathbf{w}}_{\text{visc}}, \quad (4)$$

where $\dot{\mathbf{w}}_{\text{mag}} = \nabla \times (\mathbf{J} \times \mathbf{B}/\rho)$ is the magnetically produced vorticity and $\dot{\mathbf{w}}_{\text{visc}} = \nabla \times \mathbf{F}_{\text{visc}}$ is the viscously produced vorticity. Under the assumption that $\nu = \text{const}$, we find (Mee & Brandenburg 2006)

$$\dot{\mathbf{w}}_{\text{visc}} = \nu \nabla^2 \mathbf{w} + \nu \nabla \times \mathbf{G}, \quad (5)$$

where $G_i = 2S_{ij} \nabla_j \ln \rho$ is a term that always drives vorticity—even if it is initially absent. Alternatively, if $\mu \equiv \nu \rho = \text{const}$, we have $\mathbf{F}_{\text{visc}} = \rho^{-1} \mu (\nabla^2 \mathbf{u} + \frac{1}{3} \nabla \nabla \cdot \mathbf{u})$ and

$$\dot{\mathbf{w}}_{\text{visc}} = \frac{\mu}{\rho} \left[\nabla^2 \mathbf{w} + \nabla \ln \rho \times (\nabla \times \mathbf{w} - \frac{4}{3} \nabla \nabla \cdot \mathbf{u}) \right], \quad (6)$$

when $\mu = \text{const}$. This expression shows that viscous vorticity production results from the obliqueness of density and velocity divergence gradients, which is somewhat analogous to vorticity production by a baroclinic term in the nonisothermal case. The $1/\rho$ term in the expression for $\dot{\mathbf{w}}_{\text{mag}}$ is generally only of minor importance when the Mach number is small. Thus, in the following, we focus on the case $\nu = \text{const}$, where vorticity production occurs through similar terms as in the case $\mu = \text{const}$.

While $\dot{\mathbf{w}}_{\text{visc}}$ can play a role at small scales, it is not the only term that can convert acoustic motions into vortical motions in a magnetized flow. This is because acoustic flows modify the magnetic field, which may then exert a Lorentz force with a finite curl. We refer to this as magnetically assisted vorticity production.

We give a simple one-dimensional example of this process in Sect. 3.6.1, and in Sect. 3.6.2 we present a set of simulations that validate the scaling relations obtained from the one-dimensional model.

2.3. Initial velocity field

Our study is based on the PENCIL CODE (Pencil Code Collaboration et al. 2021), which employs sixth-order centered differences and a third-order time-stepping scheme. In all cases, we use a resolution of 1024^3 mesh points. Our simulations have periodic boundary conditions, so the mass in the volume is conserved, and the mean density $\rho_0 \equiv \langle \rho \rangle$ is constant. Here and below, angle brackets denote volume averaging.

Our initial velocity and vector potential are constructed in Fourier space as $\mathbf{u}(\mathbf{x}) = \sum \tilde{\mathbf{u}}(\mathbf{k}) e^{i\mathbf{k}\cdot\mathbf{x}}$ and $\mathbf{A}(\mathbf{x}) = \sum \tilde{\mathbf{A}}(\mathbf{k}) e^{i\mathbf{k}\cdot\mathbf{x}}$ with

$$\tilde{u}_i(\mathbf{k}) = \left[(1 - \zeta) \delta_{ij} - (1 - 2\zeta) \hat{k}_i \hat{k}_j \right] u_{\text{ini}} \tilde{S}_j(\mathbf{k}), \quad (7)$$

$$\tilde{A}_i(\mathbf{k}) = \left(\delta_{ij} - \hat{k}_i \hat{k}_j \right) A_{\text{ini}} \tilde{S}_j(\mathbf{k}). \quad (8)$$

Here, u_{ini} and A_{ini} are amplitude factors, \hat{k}_i are the components of the unit vector $\hat{\mathbf{k}} \equiv \mathbf{k}/k$, $\tilde{S}_j(\mathbf{k})$ is a vector field in Fourier space with three independent components that depend on $k = |\mathbf{k}|$ but have random phases $\varphi(\mathbf{k})$ for each \mathbf{k} vector, and ζ is the irrotationality parameter with $\zeta = 0$ when the initial velocity is vortical and $\zeta = 1$ when it is acoustic (irrotational). Here, we choose

$$\tilde{S}_j(\mathbf{k}) = \frac{k_0^{-3/2} (k/k_0)^{\alpha/2-1}}{1 + (k/k_0)^{(\alpha+5/3)/2}} e^{i\varphi(\mathbf{k})}, \quad (9)$$

where k_0 is the peak wavenumber of the initial condition, and α is the slope of the subinertial range, which we set to $\alpha = 4$ in this work.

2.4. Diagnostic Quantities

An important characteristic of turbulence is its energy spectrum. The kinetic energy density per linear wavenumber interval, $E_K(k, t)$, is defined as the modulus squared of the Fourier transform of the velocity integrated over concentric shells in wavevector space. The spectrum is normalized such that $\mathcal{E}_K(t) = \int E_K(k, t) dk$ is the mean kinetic energy density. To obtain the energy per unit volume, we include a ρ_0 factor, so $\mathcal{E}_K(t) = \rho_0 \langle \mathbf{u}^2 \rangle / 2$, but we refer the reader to Kritsuk et al. (2007) for alternatives.

The magnetic energy spectrum $E_M(k, t)$ is defined analogously such that $\mathcal{E}_M(t) = \int E_M(k, t) dk$ is the mean magnetic energy density with $\mathcal{E}_M(t) = \langle \mathbf{B}^2 \rangle / 2\mu_0$. In addition, we also compute the spectrum of the vorticity,

$E_w(k, t)$, analogously to $E_K(k, t)$, but with the velocity \mathbf{u} being replaced by the vorticity $\mathbf{w} = \nabla \times \mathbf{u}$. In this case, $E_w(k, t)$ is related to the vortical part of the kinetic energy spectrum, $E_V(k, t)$, through $E_V(k, t) = E_w(k, t)/k^2$.

Finally, we also consider the scaled logarithmic density spectrum, $E_{\ln\rho}(k, t)$, which is normalized such that $\int E_{\ln\rho}(k, t) dk = \rho_0 \langle (c_s \ln\rho)^2 \rangle / 2$. Looking at Equation (1), the spatiotemporal Fourier transform of its linearized form reads $-i\omega \widetilde{\ln\rho} = -i\mathbf{k} \cdot \tilde{\mathbf{u}}$, where ω is the frequency. Using the dispersion relation for sound waves, $\omega = c_s k$, we have $c_s \ln\rho = \hat{\mathbf{k}} \cdot \tilde{\mathbf{u}}$, so that $c_s \ln\rho$ is directly a proxy for the longitudinal velocity, and $E_{\ln\rho}(k, t)$ is a proxy of the energy spectrum of the acoustic part, $E_A \approx E_{\ln\rho}$. We note that $E_K = E_V + E_A$ is a fairly accurate decomposition, at least for subsonic flows. We therefore compute the acoustic velocity spectrum as $E_A = E_K - E_V$, and have verified that $E_{\ln\rho}$ is indeed a good approximation of E_A .

The kinetic and magnetic dissipation rates are

$$\epsilon_K \equiv \langle 2\nu\rho \mathbf{S}^2 \rangle, \quad \text{and} \quad \epsilon_M \equiv \langle \eta\mu_0 \mathbf{J}^2 \rangle, \quad (10)$$

respectively. The magnetic dissipation can also be obtained from $\epsilon_M(t) = \int 2\eta k^2 E_M(k, t) dk$. For the kinetic energy dissipation, however, we have to remember that vortical and irrotational parts contribute differently, because

$$\langle \mathbf{S}^2 \rangle = \langle \mathbf{w}^2 \rangle + \frac{4}{3} \langle (\nabla \cdot \mathbf{u})^2 \rangle. \quad (11)$$

Therefore, we also define $\epsilon_V(t) = \int 2\nu k^2 E_V(k, t) dk$, and $\epsilon_A(t) = \frac{4}{3} \int 2\nu k^2 E_A(k, t) dk$, but note that, in general, $\epsilon_K \neq \epsilon_V + \epsilon_A$ owing to the existence of mixed terms.

To characterize the velocity and magnetic fields of our runs, we define five different Mach numbers. The usual Mach number is $\text{Ma} = u_{\text{rms}}/c_s$, which characterizes the combined vortical and acoustic parts. This can also be characterized separately through $\text{Ma}_V = \sqrt{2\mathcal{E}_V/\rho_0}/c_s$ and $\text{Ma}_A = \sqrt{2\mathcal{E}_A/\rho_0}/c_s$, so that $\text{Ma}^2 = \text{Ma}_V^2 + \text{Ma}_A^2$. The magnetic field is characterized by the Alfvén speed $v_A = B_{\text{rms}}/\sqrt{\rho_0\mu_0}$, which allows us to define a corresponding Mach number. Here, it is convenient to consider separately the contributions from the imposed field $v_{A0} = B_0/\sqrt{\rho_0\mu_0}$ and the rest, v_{A1} , so that $v_A^2 = v_{A0}^2 + v_{A1}^2$. The corresponding Mach numbers are then $\text{Ma}_{M0} = v_{A0}/c_s$ and $\text{Ma}_{M1} = v_{A1}/c_s$.

We also define the time-dependent Reynolds number $\text{Re} = u_{\text{rms}}\xi_K/\nu$ based on the usual integral scale:

$$\xi_K = \int k^{-1} E_K(k) dk / \mathcal{E}_K \quad (12)$$

and quote in the following a late-time average when it varies only slowly. In all cases, our Mach numbers are

Table 1. Summary of the runs discussed in this paper. Columns show the run name (column 1), irrotationality parameter ζ (column 2), induction switch ι (column 3), the normalized peak wavenumber $\tilde{k}_0 = k_0/k_1$ (column 4), the normalized amplitudes of initial random velocity and vector potential, $\tilde{u}_{\text{ini}} = u_{\text{ini}}/c_s$ and $\tilde{A}_{\text{ini}} = k_1 A_{\text{ini}}/\sqrt{\rho_0 \mu_0 c_s}$ (columns 5 and 6), five different Mach numbers (columns 7–11), the Reynolds number (column 12), and six different Kolmogorov-type parameters (columns 13–18). Dashes indicate that C_M cannot be determined for nonmagnetic runs. Run D is the same as Run C, except that the induction term has been ignored in Equation (3).

Run	input parameters						output parameters											
	ζ	ι	\tilde{k}_0	\tilde{u}_{ini}	\tilde{A}_{ini}	Ma_{M0}	Ma_{M1}	Ma_{K}	Ma_{V}	Ma_{A}	Re	C_{M}	C_{K}	C_{KV}	C_{KA}	C_{V}	C_{A}	
A	0	1	10	0.020	0	0	0	0.020	0.020	0.002	1200	—	1.62	1.62	0.00	1.65	0.00	
B	1	1	10	0.020	0	0	0	0.013	0.000	0.013	1000	—	6.06	0.00	6.06	0.35	6.06	
C	1	1	10	0.020	0.005	0	0.009	0.014	0.004	0.013	1100	2.93	6.31	0.33	5.99	0.80	7.22	
D	1	0	10	0.020	0.005	0	0.019	0.033	0.031	0.010	1200	0.00	1.86	1.65	0.22	1.69	0.48	
E	0	1	10	0	0.005	0	0.008	0.003	0.003	0.000	200	2.88	0.96	0.96	0.00	0.96	0.02	
F	1	1	10	0.020	0	1.00	0.010	0.014	0.008	0.012	200	3.66	3.92	1.57	2.35	3.09	3.17	
G	1	1	2	0.020	0.005	0	0.014	0.013	0.007	0.011	2100	1.80	6.58	0.86	5.72	1.54	7.36	
H	1	1	2	0.020	0	0	0	0.026	0.000	0.026	1300	—	2.17	0.00	2.17	0.26	2.18	
I	1	1	2	0.020	0	0.02	0	0.026	0.000	0.026	1900	0.19	2.26	0.00	2.26	0.18	2.27	
J	1	1	2	0.020	0	0.05	0.001	0.026	0.000	0.026	1900	0.35	2.26	0.00	2.26	0.32	2.28	
K	1	1	2	0.020	0	0.10	0.002	0.026	0.001	0.026	1500	0.57	2.13	0.00	2.12	0.74	2.13	
L	1	1	2	0.020	0	0.20	0.004	0.026	0.001	0.026	1300	0.98	2.11	0.02	2.09	1.39	2.09	
M	1	1	2	0.020	0	0.50	0.011	0.026	0.005	0.025	1900	1.95	2.47	0.17	2.30	2.18	2.35	
N	1	1	2	0.020	0	1.00	0.020	0.028	0.015	0.023	1900	2.92	3.13	1.01	2.12	2.32	2.67	
O	1	1	2	0.004	0	0.10	0.001	0.008	0.000	0.008	500	0.63	2.74	0.00	2.74	0.16	2.76	
P	1	1	2	0.004	0	1.00	0.006	0.008	0.004	0.007	500	2.90	3.12	0.55	2.57	1.99	2.87	

averaged over a fixed interval at a time of around one hundred sound travel times, $(c_s k_1)^{-1}$. The values of the Mach numbers are well below unity, and the magnetic Prandtl number, $\text{Pr}_M = \nu/\eta$, is taken to be unity in all cases.

It is convenient to present magnetic and kinetic energy spectra in normalized form. Instead of normalizing them by a quantity characterizing the large-scale properties (\mathcal{E}_K/k_0), we choose here to normalize them by the quantity $\epsilon_K^{2/3}/k_0^{5/3}$ characterizing the small scales. For our runs, we take the values $k_0/k_1 = 10$ and 2.

3. RESULTS

3.1. Summary of the Runs

We have performed a series of runs varying the input parameters ζ , ι , k_0 , u_{ini} , A_{ini} , Ma_{M0} , and Ma_{M1} ; see Table 1 for a summary. Nonmagnetic runs are those where $\text{Ma}_{\text{M0}} = \text{Ma}_{\text{M1}} = 0$ (see Runs A, B, and H). When $\text{Ma}_{\text{M0}} = 0$, but $\text{Ma}_{\text{M1}} \neq 0$, we have initially a random (‘turbulent’) magnetic field with a spectrum peaking at $k \approx k_0$, similar to the initial velocity field (Runs C–E and G). Run D is the same as Run C, except that the induction term has been ignored in Equation (3), i.e., $\iota = 0$. The Mach numbers are in the range 0.007–0.04, and the Reynolds number is in the range 200–1900.

The Kolmogorov-type parameter or prefactor for the magnetic field, C_M , varies significantly and is usually in the range 2–8. In all cases with $\zeta \neq 0$, C_K exceeds the typical value of 1.6 for vortical turbulence (Run A). Almost no vorticity is produced when Ma_K and C_{KV} are small (Runs B, C, H–L, and O). This is the case for all nonmagnetic and weakly magnetized cases when $\text{Ma}_{\text{M0}} \lesssim 0.1$. Vorticity is produced when $\text{Ma}_{\text{M0}} \gtrsim 0.01$ or $\text{Ma}_{\text{M1}} \gtrsim 0.02$ (Runs C–E and G). We recall that Run G has a smaller value of k_0 than Runs C–E.

3.2. Comparison of Typical Spectra

The velocity spectra for Run A, with vortical hydrodynamic turbulence, Run B, with acoustic hydrodynamic turbulence, and Run C, with acoustic MHD turbulence, are compared at a fixed time in Figure 1. We see that, although our runs have a fixed viscosity ($\nu k_1/c_s = 10^{-6}$ for $k_0/k_1 = 10$ and $\nu k_1/c_s = 5 \times 10^{-6}$ for $k_0/k_1 = 2$), and similar values for the Mach Number, only Run A has a spectrum that still possesses significant energy at large k . It is also the only run with a marked bottleneck, i.e., a shallow part just before the viscous subrange at large k (Falkovich 1994). The peak of the scaled spectra for Run B is higher, reflecting the fact that the Kolmogorov prefactor for acoustic turbulence is larger, as we discuss

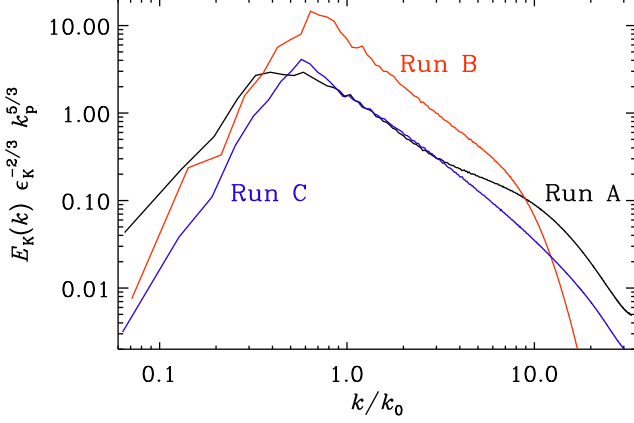


Figure 1. Kinetic energy spectra for Runs V (black), A (red), and C (blue), all at time $t = 28/c_s k_1$. No distinction between vortical and acoustic contributions has been made.

below. Finally, the kinetic energy spectra for Runs B and C are similar to that for Run A, except there is no visible bottleneck.

3.3. Kolmogorov Prefactor

In Kolmogorov's theory, the constancy of the kinetic energy flux along the turbulent cascade makes ϵ_K an important quantity for dimensional arguments. On dimensional grounds, the spectrum should be equal to $C_K \epsilon_K^{2/3} k^{-5/3}$, where C_K , the dimensionless prefactor, is the Kolmogorov constant (Frisch 1995). To obtain the value of C_K , it is convenient to present compensated spectra, $\epsilon_K^{-2/3} k^{5/3} E_K(k, t)$, which should show a constant plateau in the k range where the Kolmogorov scaling applies. Note that the difference with our normalization in Figure 1 lies in the fact that there the factor $k_0^{5/3}$ was a constant, but now it is k dependent.

We begin with the more familiar vortical case with $\zeta = 0$ and no magnetic field ($\mathbf{B} = 0$, Run A). The result is shown in Figure 2, where we see the approach to a plateau in the compensated spectrum at the level $C_K \approx 1.6$, which agrees with the usual Kolmogorov constant (Kaneda et al. 2003; Brandenburg et al. 2023). Near the dissipative subrange, we also see a strong bulge. This was already evident from Figure 1 and was characterized as the bottleneck (Falkovich 1994). It is significantly stronger here than for ordinary (stationary) turbulence, for which the compensated spectrum at the bottleneck is usually well below 3 (Kaneda et al. 2003; Haugen et al. 2004; Brandenburg et al. 2023). This could partially be a consequence of having underresolved the high wavenumbers at early times.

The corresponding case for acoustic turbulence, where $\zeta = 1$, looks different in many ways. This is shown in Figure 3, where we plot spectra that are compensated

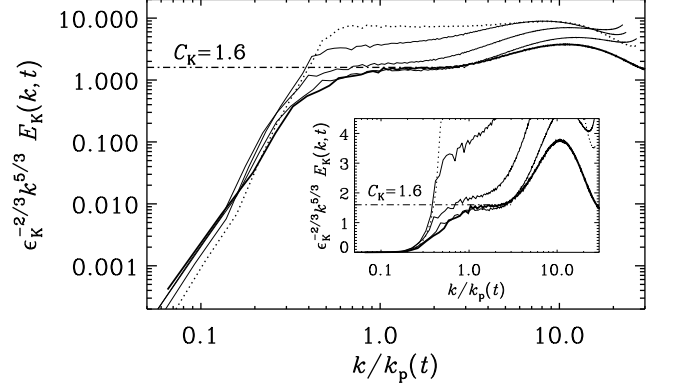


Figure 2. Compensated kinetic energy spectra for Run A at times $c_s k_1 t = 3, 7, 14$, and 28 . The dotted line denotes the initial state, and the thick line marks the last time. The dashed-dotted horizontal line marks the approach to the value $C_K = 1.5$. The inset shows the approach to a plateau in a semilogarithmic plot.

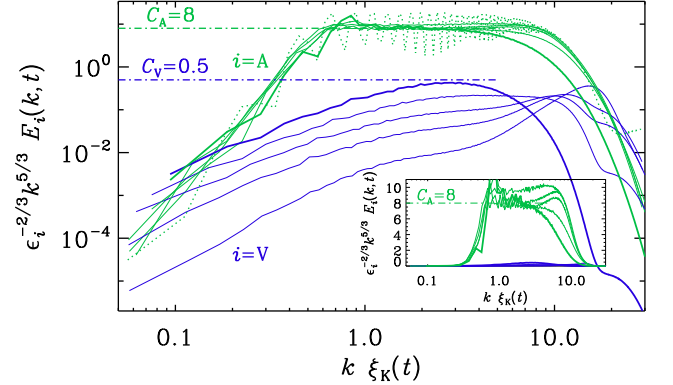


Figure 3. Compensated kinetic energy spectra for acoustic turbulence (Run B), $\epsilon_i^{-2/3}(t) k^{5/3} E_i(k, t)$, separated into the vortical ($i = V$, blue lines) and acoustic ($i = A$, green lines) components.

separately for the vortical and acoustic parts, i.e.,

$$c_i(k, t) = \epsilon_i^{-2/3}(t) k^{5/3} E_i(k, t), \quad (13)$$

and denote by C_i the approximate average of $c_i(k, t)$ over the flat part for $i = V$ or A . Here, we still see the approach to a plateau, but the bottleneck is very weak (see the inset). Instead, there is a spike in E_A at the low-wavenumber end, where the spectrum transits from the subinertial range to the inertial range. In the following, we refer to this spike as the subinertial range peak. The height of the plateau also significantly exceeds the usual value for vortical turbulence and is $C_A \approx 8$, suggesting that the standard Kolmogorov phenomenology may not be applicable.

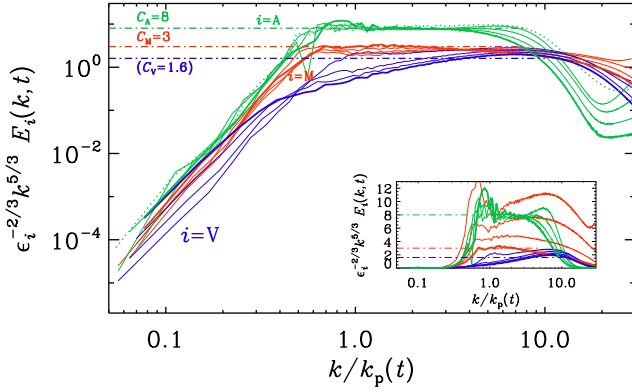


Figure 4. Similar to Figure 3, but for Run C, where the magnetic field produces vorticity. Compensated magnetic energy spectra are also plotted ($i = M$, red lines). The dashed-dotted horizontal lines indicate the approximate positions of plateaus at $C_A \approx 8$ (green), $C_M = 3$ (red), and $C_V \approx 2$ (blue).

In Run B, some vorticity is produced by the interaction with viscosity. Although the spectrum in Figure 3 is normalized by ϵ_A , the level of the plateau is low (around 0.5), although it still increases over time. As discussed in Sect. 2.1, this vorticity production results from the obliqueness of density and velocity divergence gradients. We find that the amount of vorticity production is virtually the same regardless of whether ν or μ is constant. This is likely because the Mach number is small in both cases, meaning that density fluctuations are also small.

3.4. Magnetic Vorticity Production

Next, for Run C, we consider an irrotational initial flow ($\zeta = 1$, just like Run B) together with a random initial magnetic field with a spectrum $E_M \propto k^4$ for $k < k_0$ and $E_M \propto k^{-5/3}$ for $k > k_0$, just like the initial velocity field. Depending on the relative strengths of the magnetic and velocity fields, the curl of the Lorentz force can drive vorticity through the $\dot{\mathbf{w}}_{\text{visc}}$ term in Equations (5) and (6).

The result for Run C is shown in Figure 4. Interestingly, the magnetic energy $E_M(k)$ shows neither a marked bottleneck nor a marked subinertial range peak. The compensated $c_V(k)$ spectrum of Equation (13) does not have a plateau, but it crosses $C_V \approx 1.6$ at intermediate wavenumbers. Note, however, that $C_M(t)$ has a plateau with a magnetic Kolmogorov prefactor of about 3; see Figure 4.

In the Appendix, we compare spectra for Runs C and E with and without initial turbulence, Runs C and D with and without the induction term, i.e., $\iota = 1$ and 0, respectively, as well as Runs C and G with $k_0/k_1 = 10$ and 2, respectively. We see that in Run E, turbulence

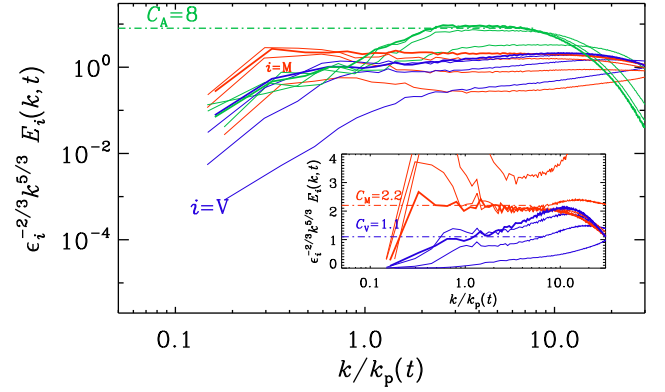


Figure 5. The same as Figure 4, but for Run G with $k_0/k_1 = 2$.

is gradually produced. Regarding the presence or absence of the induction term, we see that for Run C the induction term enables the magnetic and kinetic energy cascades to be nearly parallel. This is not the case when the induction term is absent (Run D). Finally, comparing Runs C and G, we see that for both $k/k_1 = 2$ and 10, there is a loss of kinetic energy in the acoustic components along with a gain of kinetic energy in the vortical component.

3.5. Comparison with Earlier Work

In the presence of irrotational forcing, [Kahnashvili et al. \(2012\)](#) found that, for an inflationary magnetic field with a magnetic energy spectrum proportional to k^{-1} , vortical turbulence develops with a spectrum $E_V(k)$ that is in equipartition, i.e., $E_V(k) \approx E_M(k)$. Comparing this with our present results, we see that equipartition between $E_V(k)$ and $E_M(k)$ exists only at high wavenumbers. This difference with [Kahnashvili et al. \(2012\)](#) seems to be connected with the fact that they used an inflationary magnetic field with a k^{-1} spectrum, whereas here $E_M(k)$ has a peak at intermediate wavenumbers. To further verify this interpretation, we show in Figure 5 the compensated spectra of $E_V(k, t)$ and $E_M(k, t)$ for a run with $k_0/k_1 = 2$. Here, we see that the range over which the two spectra are nearly parallel is not only increased, but also the degree of equipartition is better, i.e., the two spectra are closer together.

The velocity spectrum generated by the Lorentz force of such a magnetic field alone, i.e., without an initial acoustic component, is known to develop a shallow spectrum near k_0 , and is in approximate equipartition with the magnetic field at large wavenumbers. This is similar to the E_V spectrum in Figure 4, where the compensated spectra are proportional to $k^{2/3}$, suggesting that

$E_V(k) \propto k$ in the beginning of the magnetic inertial range.

In agreement with the earlier work of Mee & Brandenburg (2006), the present results confirm that acoustic turbulence hardly contributes to driving magnetic fields. Theoretically, small-scale dynamo action of the type first proposed by Kazantsev (1968) should also be possible for acoustic turbulence (Kazantsev et al. 1985; Martins Afonso et al. 2019), but this has never been confirmed numerically (Mee & Brandenburg 2006). What has been confirmed, however, is a small negative turbulent magnetic diffusivity (Rädler et al. 2011). Because its negative value is never larger than the positive microphysical magnetic diffusivity, it can only slow down the decay without leading to dynamo action from this effect alone. Furthermore, this negative turbulent magnetic diffusivity effect only concerns the mean or large-scale magnetic field.

3.6. Magnetically Assisted Vorticity Conversion

As we have seen from Table 1, runs with sufficiently strong uniform magnetic fields produce noticeable amounts of vorticity. Here, the mechanism causing vorticity is different from the vorticity production considered in Sect. 3.4, because it relies on the presence of initially acoustic turbulence. This is what we call magnetically assisted vorticity conversion. To gain a better understanding of this mechanism, we first consider a simple one-dimensional example.

3.6.1. Vorticity Conversion in One Dimension

The conversion of acoustic kinetic energy into vortical kinetic energy can be demonstrated with the help of a one-dimensional example. We consider a domain $-\pi < x < \pi$ with a uniform magnetic field in the diagonal direction, $\mathbf{B}_0 = (B_{0x}, B_{0y}, 0)$, constant density, $\rho = \rho_0$, and a standing sound wave initially, i.e., $u_x = u_0 \sin kx$. All the kinetic energy is in acoustic motions. The uncoupled induction equation reads $\dot{A}_z = u_x B_{0y}$, and the momentum equation becomes $\dot{\mathbf{u}} = J_z(-B_{0y}, B_{0x}, 0)/\rho_0$, where dots denote time derivatives. For vorticity production, which yields $w_z = u'_y$, where primes denote x derivatives, only the u_y component matters, and thus we have $\dot{w}_z = J'_z B_{0x}/\rho_0$. Taking another time derivative and using $J_z = -A''_z$, we have $\ddot{w}_z = -u'''_x v_{Ax} v_{Ay}$, where v_{Ax} and v_{Ay} are the Alfvén speeds in the x and y directions, respectively. Replacing t and x derivatives by factors of ω and k , and using the dispersion relation for sound waves, $\omega = c_s k$, we find for the vorticity amplitude

$$w_z = (v_{Ax} v_{Ay} / c_s^2) u_0 k. \quad (14)$$

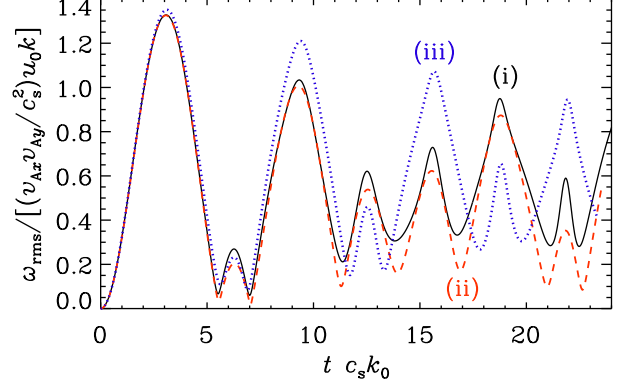


Figure 6. (i) $u_0 = 0.1$, $B_0 = 0.1$; (ii) $u_0 = 0.05$, $B_0 = 0.1$; (iii) $u_0 = 0.1$, $B_0 = 0.05$. Note that the normalized curves of w_{rms} for all three cases are initially the same.

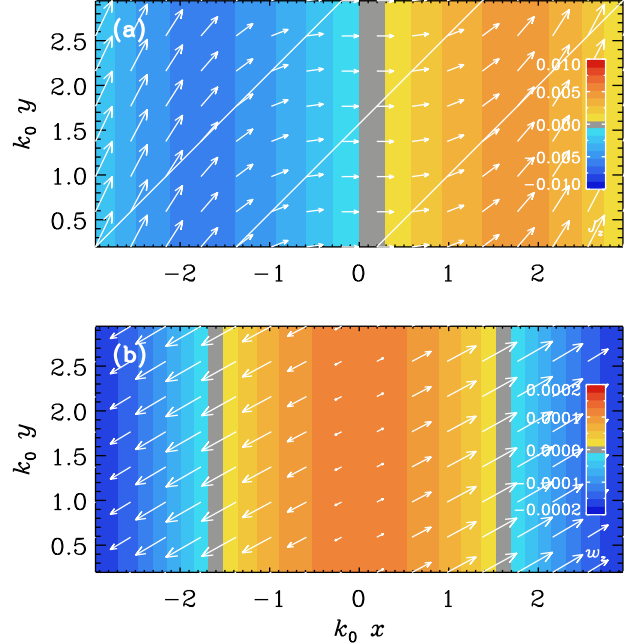


Figure 7. Visualization of (B_x, B_y) vectors overlaid on a color-scale representation of J_z (a) and of (u_x, u_y) vectors overlaid on w_z (b) in a two-dimensional plane by replicating the data of the one-dimensional calculation in the y direction.

For $u_x = u_0 \sin kx$, w_z is proportional to $\cos kx$. In Figure 6, we show three cases: (i) $u_0 = 0.1$, $B_0 = 0.1$; (ii) $u_0 = 0.05$, $B_0 = 0.1$; and (iii) $u_0 = 0.1$, $B_0 = 0.05$. We see that the linear scaling in u_0 and the quadratic scaling in B_0 in Equation (14) is reproduced by a numerical simulation of this one-dimensional initial value problem.

In Figure 7 we present visualizations of (B_x, B_y) vectors and (u_x, u_y) vectors overlaid on color-scale representations of J_z and w_z , respectively. To make the small departures from the uniform field more clearly visible,

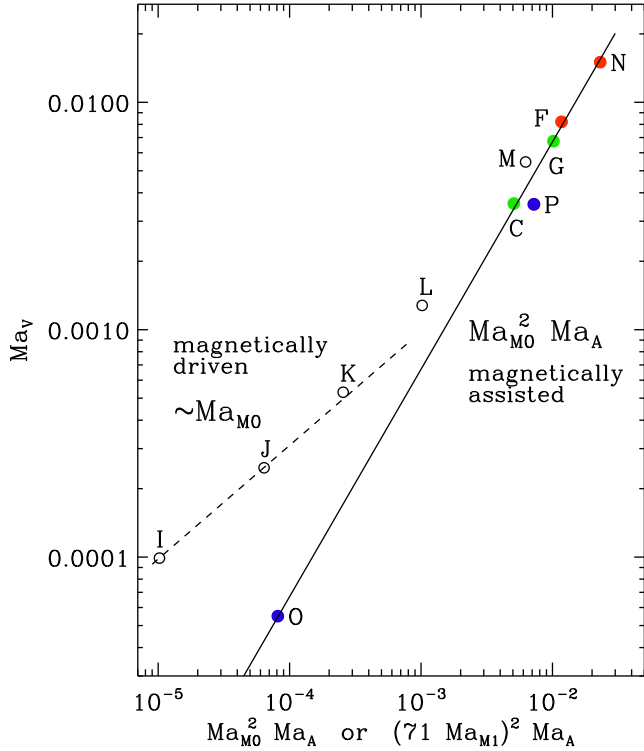


Figure 8. Dependence of Ma_V on $Ma_{M0}^2 Ma_A$ for our three-dimensional runs with an imposed magnetic field, and on $(71 Ma_{M1})^2 Ma_A$ for Runs C and G without imposed magnetic field. The red filled symbols mark Runs F and N, while the blue filled symbols mark Runs O and P. The green filled symbols mark Runs C and G without an imposed magnetic field. The solid line corresponds to $0.67 Ma_{M0}^2 Ma_A$ and the dashed line to $0.03 Ma_{M0}$. The uppercase letters denote the runs.

we have scaled the perturbations of B_y by a factor of 20 and u_y by a factor of 300.

Given that the magnetically assisted conversion of acoustic into vortical motions requires strong fields, it is of interest to see whether the strength of this conversion agrees with what is implied by Equation (14). This is done in the next section.

3.6.2. Vorticity Conversion in Three Dimensions

To see if the scaling found in Sect. 3.6.1 applies to our runs, we plot in Figure 8 the dependence of Ma_V on $Ma_{M0}^2 Ma_A$ for runs with an imposed magnetic field. Except for Runs I–L with $0.02 \leq Ma_{M1} \leq 0.2$, in which the magnetic field is weak and the acoustic turbulence strong, the vorticity obeys the expected scaling with $Ma_V \approx 0.67 Ma_{M0}^2 Ma_A$. For runs without an imposed magnetic field, the same scaling can also be recovered if we multiply Ma_{M1} by a factor of ≈ 71 , suggesting that a much weaker turbulent field has the same effect as a stronger uniform field. Note that it is difficult to dis-

tinguish this type of conversion from vorticity produced directly from the Lorentz force (here Run E). However, we see that the expected dependence on Ma_A is indeed obeyed; see Equation (14). This suggests that Runs C and G (green symbols in Figure 8) with $k_0 = 10$ and 2, respectively, and with $Ma_{M0} = 0$ and $Ma_{M1} = 0.005$ also experience magnetically assisted vorticity production.

In Figure 9, we present visualizations of $\nabla \cdot \mathbf{u}$, B^2 , and \mathbf{w}^2 on the periphery of the computational domain for Run N at three different times. We see that the structures reflect the presence of shocks extending over major parts of the domain. This is especially clear in the plots of the local vorticity density.

4. CONCLUSIONS

Acoustic turbulence is common throughout astrophysics, arising naturally from gravitational accelerations or barotropic pressure fluctuations. In this work, we have used numerical simulations to study the production of vorticity in isothermal, decaying acoustic turbulence, focusing on the role of magnetic fields.

We find that without magnetic fields, acoustic turbulence obeys a Kolmogorov-type phenomenology, with a nondimensional Kolmogorov prefactor of $C_K \approx 6$. This is significantly larger than the standard Kolmogorov constant for vortical turbulence, which is around 1.6. The presence of a magnetic field lowers this value to around 2–3 for most of our runs, although the universality of this prefactor remains uncertain, as we occasionally observe larger values.

Magnetic fields also influence the partitioning between the acoustic and vortical components of the turbulence. When a non-force-free magnetic field is added, the Lorentz force produces vorticity with a kinetic energy spectrum that is close to equipartition with the magnetic energy spectrum in the upper part of the inertial range. The turbulence also begins to resemble vortical turbulence, developing a spectrum that is nearly in equipartition with the magnetic energy spectrum at high wavenumbers. Our simulations reproduce this process, in agreement with earlier findings (Kahniashvili et al. 2012).

We also show that, even if the magnetic field is force free, it is still able to produce vorticity by converting acoustic energy into vortical kinetic energy. This conversion is most efficient when the acoustic component has significant contributions from large length scales and when the field is strong. The amplitude of the vortical component in this case is expected to scale quadratically with the magnetic field and linearly with the strength of the initial acoustic component. This scaling is confirmed by our simulations, particularly in Runs N and

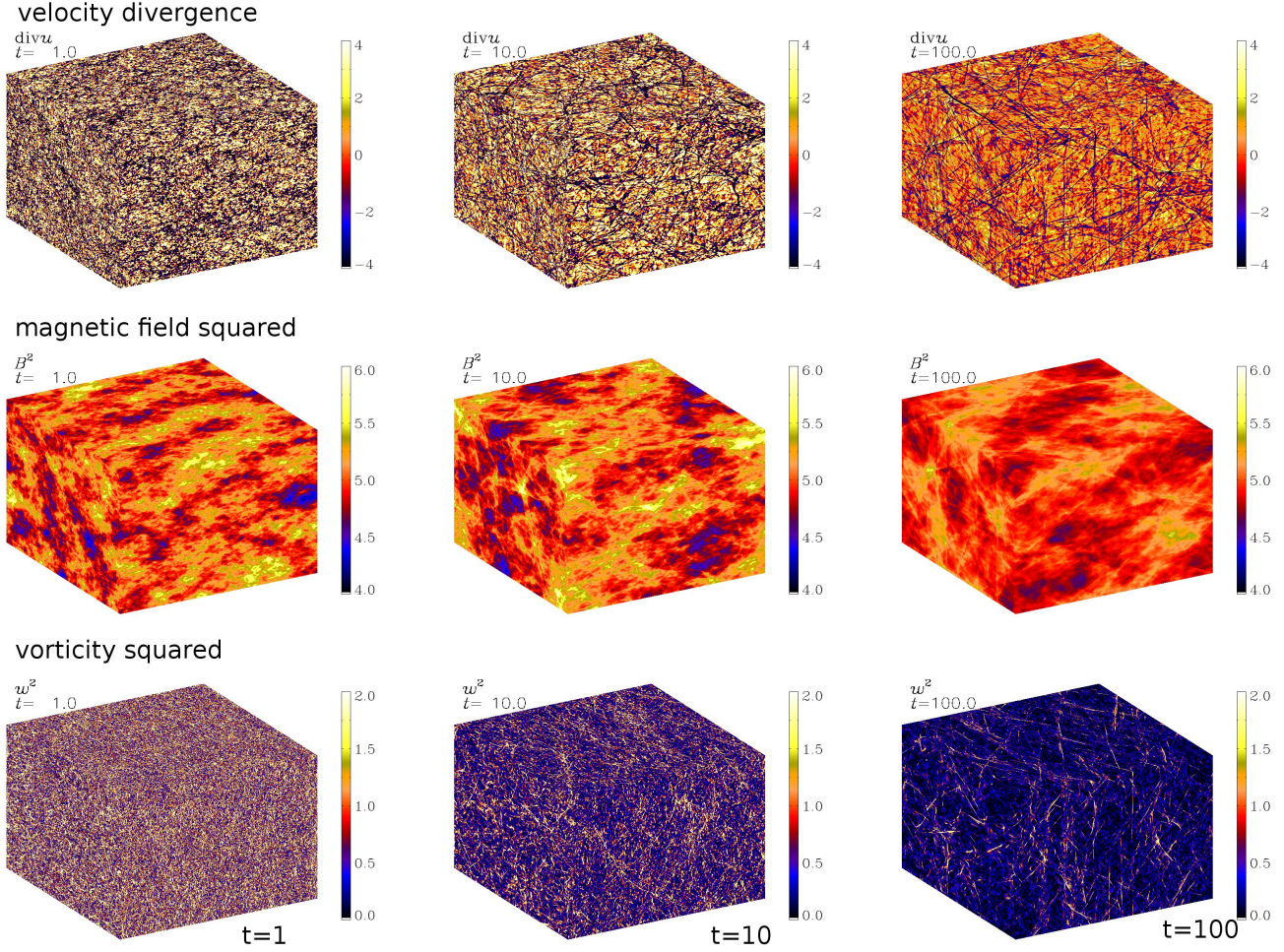


Figure 9. Visualizations of $\nabla \cdot \mathbf{u}$ (top) with a range of -4 to 4 , B^2 (middle) with a range of 4 – 6 , and w^2 (bottom) with a range of 0 to 2 . All plots are on the periphery of the computational domain for Run N at $t c_s k_1 = 1, 10$, and 100 .

P, where a strong imposed magnetic field ($\text{Ma}_{M0} = 1$) converts acoustic energy into vortical energy. Even in the case of a turbulent magnetic field, the same scaling holds, though the required field strength is much weaker ($\text{Ma}_{M1} = 0.005$).

The implications of our findings extend to cosmology, particularly to the early Universe. During the radiation-dominated era, the gas obeys an ultrarelativistic equation of state, where the pressure is proportional to the density, similar to isothermal flows. The sudden generation of acoustic turbulence, for example from cosmological phase transitions (Turner et al. 1992; Hindmarsh et al. 2015), could be converted into vortical turbulence by a magnetic field. Such a field might have been produced either during inflation or during the subsequent reheating era just prior to the radiation-dominated era. This could play a significant role in shaping the dynamics in the early Universe, particularly the generation of vortical turbulence from initially acoustic fluctuations.

We thank Liubin Pan for helpful discussions that improved the manuscript. We acknowledge inspiring discussions with the participants of the program on “Turbulence in Astrophysical Environments” at the Kavli Institute for Theoretical Physics in Santa Barbara. This research was supported in part by the Swedish Research Council (Vetenskapsrådet) under Grant No. 2019-04234, the National Science Foundation under Grants No. NSF PHY-2309135, AST-2307698, and NASA Awards 80NSSC22K0825 and 80NSSC22K1265. We acknowledge the allocation of computing resources provided by the Swedish National Allocations Committee at the Center for Parallel Computers at the Royal Institute of Technology in Stockholm.

Software and Data Availability. The source code used for the simulations of this study, the PENCIL CODE (Pencil Code Collaboration et al. 2021), is freely available on <https://github.com/pencil-code/Acoustic>. The simulation setups and corresponding input and reduced output data are freely available on <http://doi.org/10.5281/zenodo.14968754>

REFERENCES

- Beattie, J. R., Federrath, C., Kriel, N., Hew, J. K. J., & Bhattacharjee, A. 2023, arXiv e-prints, arXiv:2312.03984, doi: [10.48550/arXiv.2312.03984](https://doi.org/10.48550/arXiv.2312.03984)
- Brandenburg, A., Rogachevskii, I., & Schober, J. 2023, MNRAS, 518, 6367, doi: [10.1093/mnras/stac3555](https://doi.org/10.1093/mnras/stac3555)
- Cho, J., & Lazarian, A. 2005, ThCFD, 19, 127, doi: [10.1007/s00162-004-0157-x](https://doi.org/10.1007/s00162-004-0157-x)
- Del Sordo, F., & Brandenburg, A. 2011, A&A, 528, A145, doi: [10.1051/0004-6361/201015661](https://doi.org/10.1051/0004-6361/201015661)
- Elias-López, A., Del Sordo, F., & Viganò, D. 2023, A&A, 677, A46, doi: [10.1051/0004-6361/202346696](https://doi.org/10.1051/0004-6361/202346696)
- . 2024, A&A, 690, A77, doi: [10.1051/0004-6361/202450398](https://doi.org/10.1051/0004-6361/202450398)
- Elsasser, K., & Schamel, H. 1974, PhLA, 47, 419, doi: [10.1016/0375-9601\(74\)90155-8](https://doi.org/10.1016/0375-9601(74)90155-8)
- . 1976, ZPhyB, 23, 89, doi: [10.1007/BF01322265](https://doi.org/10.1007/BF01322265)
- Falkovich, G. 1994, PhFl, 6, 1411, doi: [10.1063/1.868255](https://doi.org/10.1063/1.868255)
- Falkovich, G., & Meyer, M. 1996, PhRvE, 54, 4431, doi: [10.1103/PhysRevE.54.4431](https://doi.org/10.1103/PhysRevE.54.4431)
- Federrath, C., Chabrier, G., Schober, J., et al. 2011, PhRvL, 107, 114504, doi: [10.1103/PhysRevLett.107.114504](https://doi.org/10.1103/PhysRevLett.107.114504)
- Federrath, C., Schober, J., Bovino, S., & Schleicher, D. R. G. 2014, ApJL, 797, L19, doi: [10.1088/2041-8205/797/2/L19](https://doi.org/10.1088/2041-8205/797/2/L19)
- Frisch, U. 1995, Turbulence. The legacy of A.N. Kolmogorov (Cambridge University Press), doi: [10.1017/CBO9781139170666](https://doi.org/10.1017/CBO9781139170666)
- Galtier, S., & Banerjee, S. 2011, PhRvL, 107, 134501, doi: [10.1103/PhysRevLett.107.134501](https://doi.org/10.1103/PhysRevLett.107.134501)
- Haugen, N. E., Brandenburg, A., & Dobler, W. 2004, PhRvE, 70, 016308, doi: [10.1103/PhysRevE.70.016308](https://doi.org/10.1103/PhysRevE.70.016308)
- Hindmarsh, M., Huber, S. J., Rummukainen, K., & Weir, D. J. 2015, PhRvD, 92, 123009, doi: [10.1103/PhysRevD.92.123009](https://doi.org/10.1103/PhysRevD.92.123009)
- Jahanbakhshi, R., Vaghefi, N. S., & Madnia, C. K. 2015, PhFl, 27, 105105, doi: [10.1063/1.4933250](https://doi.org/10.1063/1.4933250)
- Kadomtsev, B. B., & Petviashvili, V. I. 1973, SPhD, 18, 115
- Kahniashvili, T., Brandenburg, A., Campanelli, L., Ratra, B., & Tevzadze, A. G. 2012, PhRvD, 86, 103005, doi: [10.1103/PhysRevD.86.103005](https://doi.org/10.1103/PhysRevD.86.103005)
- Kaneda, Y., Ishihara, T., Yokokawa, M., Itakura, K., & Uno, A. 2003, PhFl, 15, L21, doi: [10.1063/1.1539855](https://doi.org/10.1063/1.1539855)
- Kazantsev, A. P. 1968, JETP, 26, 1031
- Kazantsev, A. P., Ruzmaikin, A. A., & Sokolov, D. D. 1985, ZhETF, 61, 285
- Kochurin, E. A., & Kuznetsov, E. A. 2022, JETPL, 116, 863, doi: [10.1134/S0021364022602494](https://doi.org/10.1134/S0021364022602494)
- Kritsuk, A. G., Norman, M. L., Padoan, P., & Wagner, R. 2007, ApJ, 665, 416, doi: [10.1086/519443](https://doi.org/10.1086/519443)
- Kuznetsov, E., & Krasnoselskikh, V. 2008, PhPl, 15, 062305, doi: [10.1063/1.2928160](https://doi.org/10.1063/1.2928160)
- L'vov, V. S., & Mikhailov, A. V. 1981, PhyD, 2, 224, doi: [10.1016/0167-2789\(81\)90076-2](https://doi.org/10.1016/0167-2789(81)90076-2)
- Martins Afonso, M., Mitra, D., & Vincenzi, D. 2019, RSPSA, 475, 20180591, doi: [10.1098/rspa.2018.0591](https://doi.org/10.1098/rspa.2018.0591)
- Mee, A. J., & Brandenburg, A. 2006, MNRAS, 370, 415, doi: [10.1111/j.1365-2966.2006.10476.x](https://doi.org/10.1111/j.1365-2966.2006.10476.x)
- Passot, T., & Pouquet, A. 1987, JFM, 181, 441, doi: [10.1017/S0022112087002167](https://doi.org/10.1017/S0022112087002167)
- Pencil Code Collaboration, Brandenburg, A., Johansen, A., et al. 2021, JOSS, 6, 2807, doi: [10.21105/joss.02807](https://doi.org/10.21105/joss.02807)
- Porter, D. H., Jones, T. W., & Ryu, D. 2015, ApJ, 810, 93, doi: [10.1088/0004-637X/810/2/93](https://doi.org/10.1088/0004-637X/810/2/93)
- Rädler, K.-H., Brandenburg, A., Del Sordo, F., & Rheinhardt, M. 2011, PhRvE, 84, 046321, doi: [10.1103/PhysRevE.84.046321](https://doi.org/10.1103/PhysRevE.84.046321)
- Ricard, G., & Falcon, E. 2023, PhRvF, 8, 014804, doi: [10.1103/PhysRevFluids.8.014804](https://doi.org/10.1103/PhysRevFluids.8.014804)
- Schleicher, D. R. G., Schober, J., Federrath, C., Bovino, S., & Schmidt, W. 2013, NJPh, 15, 023017, doi: [10.1088/1367-2630/15/2/023017](https://doi.org/10.1088/1367-2630/15/2/023017)
- Shivamoggi, B. K. 1992, PhLA, 166, 243, doi: [10.1016/0375-9601\(92\)90371-R](https://doi.org/10.1016/0375-9601(92)90371-R)
- Sreenivasan, K. R. 1995, PhFl, 7, 2778, doi: [10.1063/1.868656](https://doi.org/10.1063/1.868656)
- Turner, M. S., Weinberg, E. J., & Widrow, L. M. 1992, PhRvD, 46, 2384, doi: [10.1103/PhysRevD.46.2384](https://doi.org/10.1103/PhysRevD.46.2384)

APPENDIX

At the end of Sect. 3.4, we mentioned spectral comparisons of Run C with three other runs (Runs E, D, and G). In Figure 10, we compare the kinetic and magnetic energy spectra for Runs C and E, i.e., with and without initial turbulence. We see that turbulence is gradually generated by the magnetic field, but there is hardly any effect on the magnetic energy spectra.

In Figure 11, we show the resulting spectra for a case where the induction term, $\mathbf{u} \times \mathbf{B}$, has been suppressed in Equation (3), i.e., $\iota = 0$, and we just solve the diffusion equation, $\partial \mathbf{A} / \partial t = \eta \nabla^2 \mathbf{A}$. The magnetic field then decays preferentially at high wavenumbers, where magnetic diffusion is the strongest. This is evident from a premature cutoff of the magnetic energy spectrum. The vortical part of the kinetic energy spectrum now seems to show a very strong bottleneck, but the acoustic part does have a plateau at a low level and a small bottleneck. This suggests that the initial energy in the acoustic component is unimportant for the dynamics of the magnetic field. Moreover, the vorticity production by the magnetic field is largely independent of the initial energy in the irrotational component.

In Figure 12, we compare magnetic and kinetic energy spectra for the vortical and acoustic components

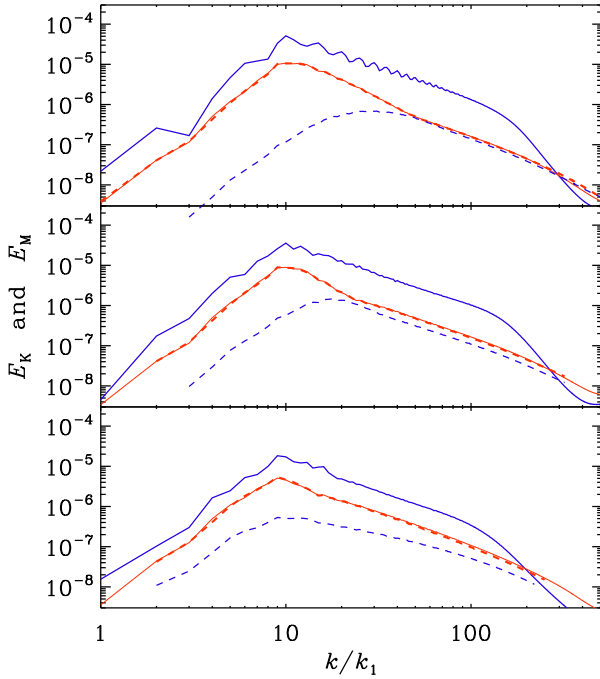


Figure 10. Comparison of kinetic (blue lines) and magnetic (red lines) energy spectra for Runs C (solid lines) and E (dashed lines), runs with and without initial turbulence, at times 2.5, 7.5, and 25.

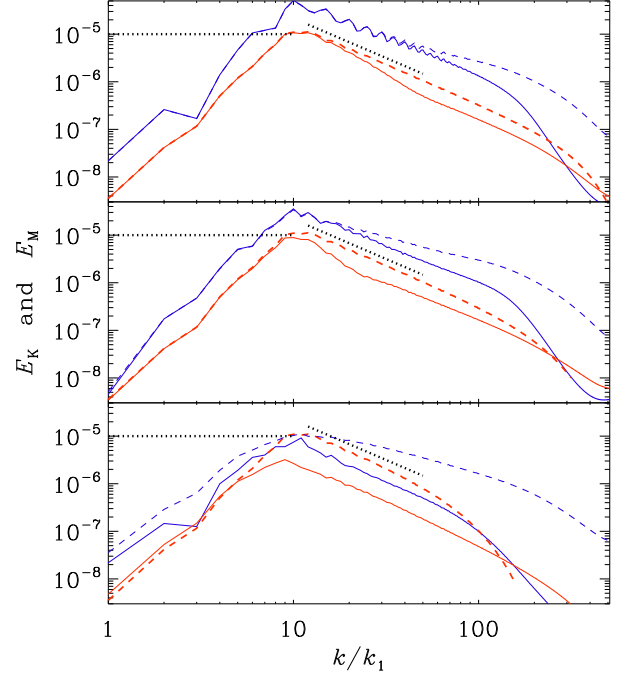


Figure 11. Similar to Figure 10, but for Runs C (solid lines) and D (dashed lines, $\iota = 0$, i.e., no induction) at times 2.5, 7.5, and 60. The black dotted lines provide fixed reference values in each panel.

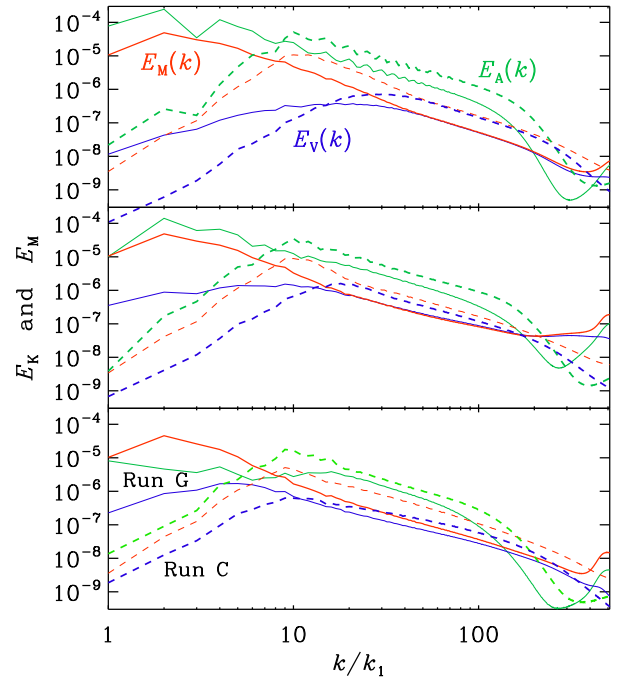


Figure 12. Comparison of acoustic (green lines), vortical kinetic (blue lines), and magnetic (red lines) energy spectra for Runs C (dashed lines) and G (solid lines) at times 2.5, 7.5, and 25.

for Runs C with G at three different times. We see that, at later times, Run G suffers a loss of kinetic energy in the acoustic components along with a gain of kinetic energy in the vortical component. This energy exchange occurs around the wavenumber $k/k_1 = 2$.